ISIJ International, Vol. 60 (2020), No. 5, pp. 876–886

# Effects of the Bulk $Fe_2O_3$ Concentration on the Controlled Solidification of "$Fe_2O_3$"–CaO–$SiO_2$ Liquids in Air

Stuart NICOL,* Evgueni JAK and Peter HAYES

Pyrometallurgy Innovation Centre (Pyrosearch), School of Chemical Engineering, The University of Queensland, Brisbane, 4072 Australia.

(*Received on August 15, 2019; accepted on November 7, 2019*)

The solidification of "$Fe_2O_3$"–CaO–$SiO_2$ liquids in air at a controlled cooling rate of 2.0 K/s for a range of $Fe_2O_3$ concentrations in the bulk has been investigated. The compositions investigated were selected such that the bulk compositions were within the hematite primary phase field and had a CaO/$SiO_2$ ratio of 3.46 wt/wt.

Non-equilibrium phase assemblages were formed for all bulk compositions investigated. Specifically, the silico ferrite of calcium (SFC) phase was not formed on cooling. The microstructures and proportions of the phase assemblages formed were found to vary with the $Fe_2O_3$ concentration in the bulk.

KEY WORDS: iron ore sinter; microstructure; solidification; "$Fe_2O_3$"–CaO–$SiO_2$; hematite.

## 1. Introduction

The local bulk iron oxide concentrations in iron ore sinters can vary as a result of a range of factors; differences in the ore characteristics, such as source, grade, physical structure and heterogeneity within the packed bed due to granulation practice, distribution of other feeds, fluxes, return sinter and secondary oxides.

An improved understanding of the impact of the bulk iron concentration on the solidification processes taking place during sintering would be beneficial in assessing the impacts of this variability on the sinter phases and microstructures. In turn, this information can be taken into account when designing granulation and operating sintering processes.

The dominant iron oxide phases in sinter, hematite and magnetite, have been observed to form a range of different morphologies and phase associations within a single sinter sample.[1)] These oxides have been broadly classified as primary, secondary and multi-component. The primary or relict hematite is the iron oxide material that is not dissolved during sintering, while the secondary hematite is formed on cooling the liquid[1)] and oxidation of magnetite during cooling. The primary hematite is typically present as euhedral crystals or is granular in morphology, and the secondary hematite in the presence of liquid forms skeletal and rhomohedral crystals. It has been postulated that the different iron oxide morphologies and phase associations result in different sinter properties.[1)]

A series of studies have been undertaken to determine the stages and phase assemblages occurring during the solidification of "$Fe_2O_3$"–CaO–$SiO_2$ melts[2,3)] and the effects of cooling rate on the phases formed and the resulting microstructures on solidification of these melts.[4)]

In the present study, a systematic investigation of the effects of changing bulk $Fe_2O_3$ concentration, independent of other controllable parameters, on the microstructures and phases formed on cooling "$Fe_2O_3$"–CaO–$SiO_2$ melts at conditions relevant to iron ore sintering is described.

## 2. Experimental Technique

Details of the experimental technique used in this study have been reported in a previous publication by the authors.[2)] The technique enables each stage of the solidification process to be identified and differentiated from the processes occurring during heating. The ability to rapidly quench the sample and to accurately capture the microstructures and phase compositions present at temperature are critical to the experimental design. The controlled cooling rates achievable with the new experimental technique are within the range of cooling rates measured in industrial iron ore sintering.[5)]

A pelletised oxide powder mixture (0.1 g, 6 mm diameter) supported on a substrate (70/30 Pt/Rh wire, 0.5 mm diameter) is heated and cooled in air in an electrically heated vertical tube furnace (alumina reaction tube, 38 mm OD 30 mm ID). The sample is vertically suspended within the reaction tube in the furnace from an alumina rod. The vertical position of the alumina rod, and in hence the position of the sample, is controlled with a positioning motor affixed to the top of the furnace. The sample is raised into the hot zone of the furnace, and the sample is held for four minutes at or above 1 623 K (1 350°C) for melting and homogenisation. After homogenisation, the sample is lowered down through the furnace with the use of a computer controlled motor drive to achieve a constant cooling rate. On reaching the target temperature the sample is quenched into water by releasing the sample, which falls under gravity into the quenching medium. The experimental apparatus is shown in **Fig. 1**.

* Corresponding author: E-mail: stuart.nicol@uqconnect.edu.au
DOI: https://doi.org/10.2355/isijinternational.ISIJINT-2019-502

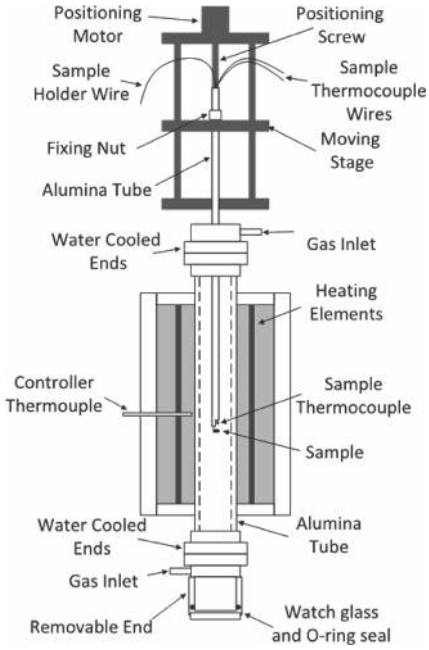


**Fig. 1.** Schematic diagram of the experimental apparatus for the controlled cooling of oxide liquids. Reproduced from Nicol.[2)]

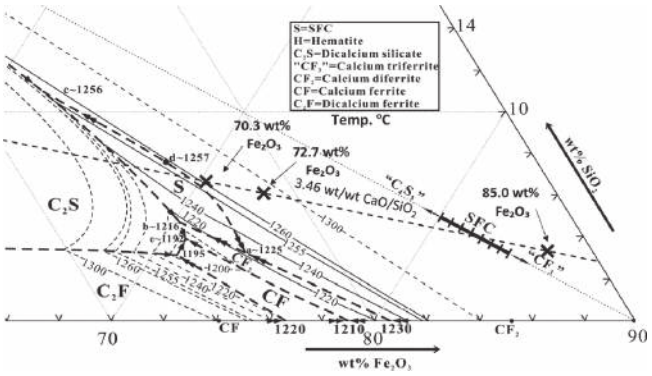


**Fig. 2.** Liquidus surface and bulk oxide compositions investigated (marked X) in the "$Fe_2O_3$"–CaO–$SiO_2$ system in air.

The quenched samples are characterised initially using optical microscopy for phase and microstructure identification using a reflected light microscope (Olympus Provis AX70TRF) and scanning electron microscopy (SEM) in back scattered electron mode (BSE). Phase compositions were measured by an electron probe X-ray microanalysis (EPMA) technique with wavelength dispersive spectroscopy (WDS) (JEOL 8200L EPMA; Japan Electron Optics Ltd., Tokyo, Japan). The EPMA was operated at a voltage of 15 keV and beam current of 20 nA. Three standards were used for calibration, pure $CaSiO_3$, $Fe_2O_3$, and $Al_2O_3$ (all standards from the Charles M. Taylor Co., Stanford, CA). The iron concentration in phases were recalculated to $Fe_2O_3$ for presentation purposes.

The phases present in the samples were confirmed with X-Ray Powder Diffraction (XRD). To enable these samples to be characterised, repeated experiments, cooling from 1 623 K to 1 073 K (1 350°C to 800°C) at 2 K/s, with 0.2 g of starting oxides were performed to obtain 1.5 g of material. The material was crushed and ground with an agate mortar and pestle. The resulting powder was analysed with powder X-Ray Diffraction (XRD) (Bruker D8), with a copper K$\alpha$ radiation source at a voltage of 40 kV and a current of 40 mA. The XRD pattern obtained between 5° and 15° 2$\theta$ were used to identify the phases present by comparison with known XRD patterns.

Three bulk oxide compositions were selected for investigation, 70.3 wt% $Fe_2O_3$ 72.7 wt% $Fe_2O_3$[2)] and 85.0 wt% $Fe_2O_3$, all with a $CaO/SiO_2$ ratio of 3.46 wt/wt; these bulk compositions are marked in **Fig. 2**. The compositions were selected such that all were within the hematite primary phase field and at this $CaO/SiO_2$ ratio, it is anticipated that the silico ferrite of calcium (SFC) phase would form on equilibrium solidification at approximately 1 529 K (1 256°C). Two compositions (70.3 wt% $Fe_2O_3$, 72.7 wt% $Fe_2O_3$) have a liquidus temperature of below 1 623 K (1 350°C), while the third (85.0 wt% $Fe_2O_3$) has a liquidus temperature of approximately 1 660 K (1 385°C). At the peak temperature of 1 623 K (1 350°C), the samples containing 85 wt% $Fe_2O_3$ in the bulk, from the phase diagram, are estimated to consist of 23 wt% hematite and 77 wt% liquid.

To provide a clear understanding of the sequences of reactions and processes occurring, a series of experiments were performed. These experiments were undertaken with samples cooled in air from the same starting temperature (1 623 K) and the same cooling rate (2 K/s); the samples were then quenched from selected temperatures between 1 533 K and 1 453 K (1 250°C and 1 180°C).

The following sequence of solidification is predicted to occur for all three compositions under Scheil-Gulliver cooling; on cooling to 1 529 K (1 256°C) the hematite primary phase is formed, from 1 529 K (1 256°C) to 1 508 K (1 235°C) SFC solidifies from the melt as it moves through the SFC primary phase field, the concurrent SFC and $C_2S$ solidification occurs from 1 508 K (1 235°C) to 1 489 K (1 216°C) with the melt following the SFC-$C_2S$ boundary line, the concurrent solidification of $CF_2$ and $C_2S$ occurs from 1 489 K (1 216°C) and 1 465 K (1 192°C) with the melt following the $CF_2$–$C_2S$ boundary line and at 1 465 K (1 192°C) the concurrent solidification of $CF_2$, CF and $C_2S$ such that below this temperature no liquid remains.

The experiments were performed in air, as the effective oxygen partial pressures present in sinter on cooling from the peak bed temperatures to the solidus (approximately 1 200°C) in iron ore sinter pot tests has been measured to be close to 0.21 atm[5)] and phase equilibria data is available for the "$Fe_2O_3$"–CaO–$SiO_2$ system in air.[6)] Samples were cooled from 1 623 K to 1 073 K at 2 K/s, with the cooling rate selected as this is typical of that encountered in industrial iron ore sintering processes.

## 3. Results

Initial experiments were undertaken with the three bulk compositions, cooled at 2 K/s from 1 623 K to 1 073 K (1 350°C to 800°C). Within this temperature range and cooling rate range, complete solidification was found to have taken place for all compositions investigated. Examples of the typical phases and microstructures formed under the cooling conditions investigated is given in **Figs. 3** and **4**.

Using FE-SEM and EPMA measurements, the phases present in the samples were identified. In all samples, hematite (H, $Fe_2O_3$), dicalcium silicate ($C_2S$, $2CaO.SiO_2$), calcium ferrite

(CF, $CaO.Fe_2O_3$) and calcium diferrite ($CF_2$, $CaO.2Fe_2O_3$) were present. In addition, samples with a bulk composition containing 70.3 wt% $Fe_2O_3$ were also found to contain both the SFCA-I and $Ca_{7.2}Fe^{2+}_{0.8}Fe^{3+}_{30}O_{53}$ phases. These two phases were determined as being present as a result of both EPMA and XRD measurements, with further details provided in Section 3.6. For simplicity, the SFCA-I and $Ca_{7.2}Fe^{2+}_{0.8}Fe^{3+}_{30}O_{53}$ phases are hereafter referred to as 'SFC-I'.

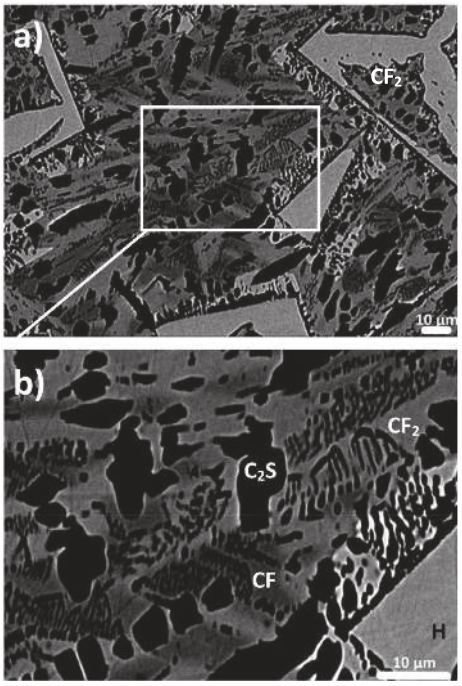


**Fig. 3.** a) Typical example of final solidified structure (1 523 K to 1 478 K, 0.5 K/s in air, 72.7 wt% $Fe_2O_3$ and $CaO/SiO_2$ ratio of 3.46 wt/wt) cooling in air at 2 K/s. (H - hematite, $C_2S$ - $2CaO.SiO_2$, $CF_2$ – $CaO.2Fe_2O_3$, CF – $CaO.Fe_2O_3$), b) detail of a) (Backscattered electron (BSE) micrographs).

The phases present in the solidified samples differ from those anticipated under both equilibrium and Scheil-Gulliver cooling. SFC was not present in any of the microstructures formed. Hematite was present in samples containing 85.0 wt% and 70.3 wt% $Fe_2O_3$ in the bulk.

Between the initial state and the final microstructure, the four intermediate stages of solidification were consistently observed for all three bulk compositions. These stages are as follows, liquid+H (Assemblage I), liquid+H+$C_2S$ (Assemblage II), liquid+$C_2S$+$CF_2$ (Assemblage III) and finally $C_2S$+$CF_2$+CF (Assemblage IV). With a bulk composition containing 70.3 wt% $Fe_2O_3$, two additional phase assemblages were observed, liquid+'SFC-I' (Assemblage V) and liquid+'SFC-I'+$C_2S$/liquid+$CF_2$+$C_2S$ (Assemblage VI). In the regions containing 'SFC-I', Assemblage IV was observed to form following Assemblage VI. The phase assemblages containing 'SFC-I' formed in regions free of hematite. As such, the formation of assemblage of V and VI is considered independent of assemblages I, II and III. The temperatures at which the different phase assemblages were observed are illustrated in **Fig. 5**.

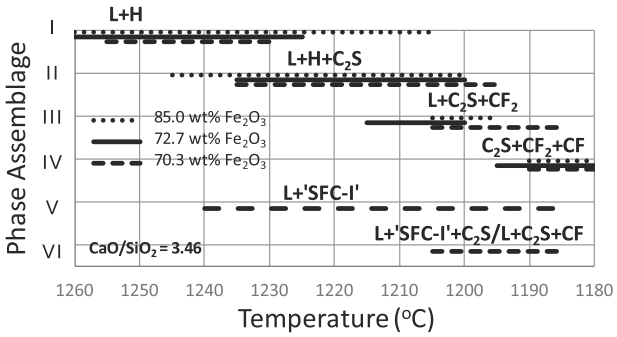


**Fig. 5.** Occurrence of assemblages with temperature during liquid solidification of "$Fe_2O_3$"–CaO–$SiO_2$ melts in air at 2 K/s ($CaO/SiO_2$ – 3.46 wt/wt).

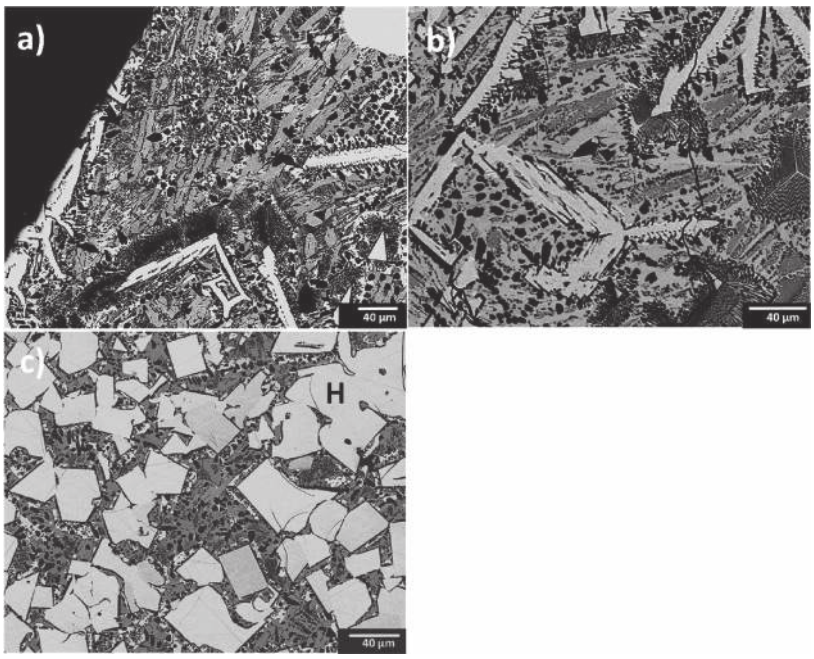


**Fig. 4.** Examples of typical microstructures observed in samples having a $CaO/SiO_2$ = 3.46 wt/wt, cooled in air at 2 K/s from 1 623 K (1 350°C) with a) 70.3 wt% $Fe_2O_3$ to 1 073 K (800°C), b) 72.7 wt% $Fe_2O_3$ to 1 468 K (1 195°C) and c) 85.0 wt% $Fe_2O_3$ to 1 468 K (1 195°C) (Backscattered Electron (BSE) Micrograph) (H-Hematite, $C_2S$ – $Ca_2SiO_2$, CF – $CaFe_2O_4$, $CF_2$ – $CaFe_4O_7$, S – 'SFC-I').

### 3.1. Liquid Composition Variation with Temperature and Bulk $Fe_2O_3$ Concentration

In the current study, the compositions of the liquids at selected temperatures were measured with EPMA, with the measured liquid compositions shown in **Fig. 6** and given in **Tables 1**, **2** and **3**. For all bulk $Fe_2O_3$ compositions studied, the same trends in liquid composition during cooling were observed.

The initial solidification of isolated hematite (Assemblage I) resulted in the liquid composition moving through the hematite and SFC primary phase fields and into the $C_2S$ primary phase field. In regions isolated from hematite, only present when the bulk composition was low in $Fe_2O_3$, the SFC-I (Assemblage V) was observed to form part way through the solidification of hematite (Assemblage I). During the formation of 'SFC-I', the liquid composition in these

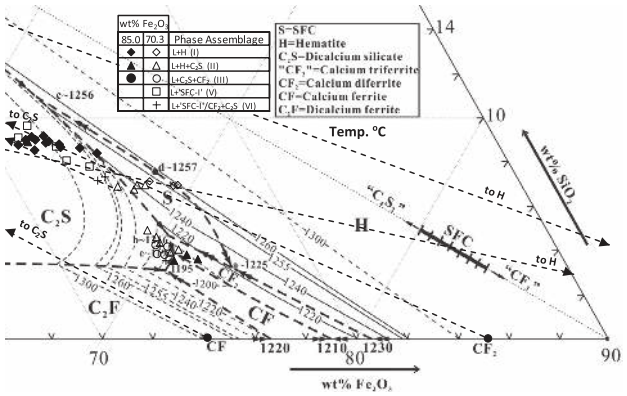


**Fig. 6.** Measured liquid compositions for oxide samples, with 85 wt%, 72.7 wt% and 70.3 wt% $Fe_2O_3$ in the bulk system, cooled from 1 623 K (1 350°C) at 2 K/s in comparison to the equilibrium liquidus for the "$Fe_2O_3$"–CaO–$SiO_2$ system in air.[6]

**Table 1.** Liquid compositions in microstructures containing Hematite, as measured by EPMA, formed by cooling a liquid with 70.3 wt% $Fe_2O_3$ from 1 623 K (1 350°C) at 2 K/s.

| Temperature (°C) | Assemblage I (L+H) | | | Assemblage II (L+H+$C_2S$) | | | Assemblage III (L+$C_2S$+$CF_2$) | | |
|---|---|---|---|---|---|---|---|---|---|
| | $Fe_2O_3$ (wt%) | $SiO_2$ (wt%) | CaO (wt%) | $Fe_2O_3$ (wt%) | $SiO_2$ (wt%) | CaO (wt%) | $Fe_2O_3$ (wt%) | $SiO_2$ (wt%) | CaO (wt%) |
| 1 260 | – | – | – | – | – | – | – | – | – |
| 1 255 | 69.2 | 6.9 | 23.8 | – | – | – | – | – | – |
| 1 250 | 69.4 | 7.0 | 23.7 | – | – | – | – | – | – |
| 1 245 | 69.4 | 6.8 | 23.7 | – | – | – | – | – | – |
| 1 240 | 69.2 | 7.0 | 23.8 | – | – | – | – | – | – |
| 1 235 | – | – | – | 69.2 | 7.1 | 23.7 | – | – | – |
| 1 230 | 68.2 | 7.2 | 24.7 | 67.7 | 6.8 | 25.5 | – | – | – |
| 1 225 | – | – | – | 68.1 | 7.0 | 24.9 | – | – | – |
| 1 220 | – | – | – | 67.8 | 7.0 | 25.2 | – | – | – |
| 1 215 | – | – | – | 70.6 | 3.9 | 25.5 | – | – | – |
| 1 210 | – | – | – | 67.0 | 6.9 | 26.0 | – | – | – |
| 1 205 | – | – | – | 70.0 | 4.3 | 25.7 | 69.9 | 4.2 | 25.9 |
| 1 200 | – | – | – | 69.7 | 4.6 | 25.7 | – | – | – |
| 1 195 | – | – | – | 69.2 | 4.9 | 25.9 | 70.4 | 4.1 | 25.5 |
| 1 190 | – | – | – | 70.9 | 4.0 | 25.1 | 70.1 | 3.8 | 26.0 |
| 1 185 | – | – | – | – | – | – | 70.4 | 3.8 | 25.8 |

**Table 2.** Liquid compositions in microstructures containing Hematite, as measured by EPMA, formed by cooling a liquid with 85.0 wt% $Fe_2O_3$ from 1 623 K (1 350°C) at 2 K/s.

| Temperature (°C) | Assemblage I (L+H) | | | Assemblage II (L+H+$C_2S$) | | | Assemblage III (L+$C_2S$+$CF_2$) | | |
|---|---|---|---|---|---|---|---|---|---|
| | $Fe_2O_3$ (wt%) | $SiO_2$ (wt%) | CaO (wt%) | $Fe_2O_3$ (wt%) | $SiO_2$ (wt%) | CaO (wt%) | $Fe_2O_3$ (wt%) | $SiO_2$ (wt%) | CaO (wt%) |
| 1 260 | 63.7 | 8.8 | 27.4 | – | – | – | – | – | – |
| 1 255 | 63.3 | 9.0 | 27.7 | – | – | – | – | – | – |
| 1 250 | 62.9 | 9.2 | 27.9 | – | – | – | – | – | – |
| 1 245 | 60.8 | 9.8 | 29.4 | – | – | – | – | – | – |
| 1 240 | 64.6 | 8.7 | 26.7 | – | – | – | – | – | – |
| 1 235 | 65.4 | 8.4 | 26.1 | – | – | – | – | – | – |
| 1 230 | 63.2 | 8.9 | 27.9 | – | – | – | – | – | – |
| 1 225 | 63.9 | 8.7 | 27.4 | – | – | – | – | – | – |
| 1 220 | 62.5 | 9.2 | 28.4 | – | – | – | – | – | – |
| 1 215 | 62.7 | 9.0 | 28.3 | 71.3 | 3.8 | 24.9 | – | – | – |
| 1 210 | 62.3 | 9.1 | 28.6 | 62.4 | 9.0 | 28.6 | – | – | – |
| 1 205 | 62.9 | 8.6 | 28.5 | 62.5 | 8.9 | 28.6 | – | – | – |
| 1 200 | 62.1 | 8.8 | 29.0 | 71.9 | 3.6 | 24.6 | – | – | – |
| 1 195 | – | – | – | 71.0 | 3.5 | 25.5 | – | – | – |

regions also moved through the SFC primary phase field and into the $C_2S$ primary phase field. At the conclusion of Assemblages I and V, the liquid composition was observed to be within the $C_2S$ primary phase field. Once $C_2S$ formed, resulting in the occurrence assemblages II ($L+H+C_2S$) and VI ($L+C_2S$ +'SFC-I'/$L+C_2S$ $+CF_2$), the liquid composition moved towards the $CF_2$ primary phase field with decreasing temperature. This solidification of $C_2S$, Hematite and/or 'SFC-I' continued until the liquid reached the $CF_2$ primary phase field. With the nucleation of $CF_2$, assemblage III ($L+C_2S$ $+CF_2$) is formed. The final phase assemblage, $C_2S+CF_2+CF$, formed after assemblages III and VI. The relationship between the sequence of formation of the six phase assemblages is shown in **Fig. 7**.

**Table 3.** Liquid compositions in microstructures containing 'SFC-I', as measured by EPMA, formed by cooling a liquid with 70.3 wt% $Fe_2O_3$ from 1 623 K (1 350°C) at 2 K/s.

| Temperature (°C) | Assemblage V (L+'SFC-I') | | | Assemblage VI (L+'SFC-I'/$CF_2$+$C_2S$) | | |
|---|---|---|---|---|---|---|
| | $Fe_2O_3$ (wt%) | $SiO_2$ (wt%) | CaO (wt%) | $Fe_2O_3$ (wt%) | $SiO_2$ (wt%) | CaO (wt%) |
| 1 240 | 62.0 | 9.1 | 28.9 | – | – | – |
| 1 235 | 60.9 | 9.5 | 29.6 | – | – | – |
| 1 230 | – | – | – | – | – | – |
| 1 225 | 65.5 | 7.8 | 26.7 | – | – | – |
| 1 220 | – | – | – | – | – | – |
| 1 215 | | | | – | – | – |
| 1 210 | – | – | – | – | – | – |
| 1 205 | 63.7 | 8.7 | 27.6 | 70.1 | 4.2 | 25.7 |
| 1 200 | 62.1 | 9.7 | 28.2 | 66.1 | 7.2 | 26.7 |
| 1 195 | – | – | – | 66.3 | 7.3 | 26.4 |
| 1 190 | – | – | – | 70.6 | 3.5 | 25.8 |
| 1 185 | 64.4 | 8.1 | 27.5 | – | – | – |

The phases and microstructures obtained on solidification differed to those predicted under equilibrium and Scheil Gulliver cooling, specifically;

- SFC was not formed in any of the samples investigated
- Liquid undercooling occurred prior to the nucleation of phases
- The peritectic reactions (L+H→L+SFC, L+SFC→L+$CF_2$) did not take place
- 'SFC-I' was observed to form on solidification of a melt with 70.3 wt% $Fe_2O_3$ in the bulk
- The solidification sequences and microstructures formed are dependent on the pre-existing phases

### 3.2. Liquid + Hematite (Assemblage I)

The formation of hematite, assemblage I (L+H), was the first phase assemblage observed on cooling, for all compositions investigated in the present study. **Figure 8** shows micrographs of the typical hematite primary phase microstructures. At a high bulk $Fe_2O_3$ composition (85 wt%), Assemblage I was observed to transition to assemblage II at lower temperatures, down to 1 478 K (1 205°C), compared

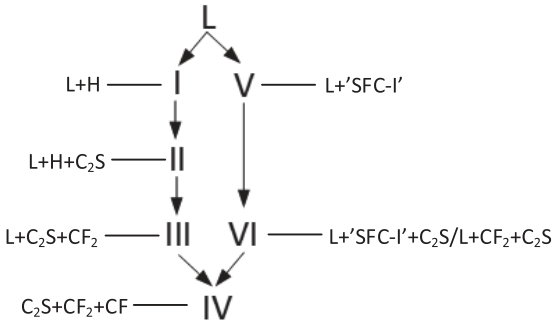


**Fig. 7.** Observed sequences of phase assemblage formation from "$Fe_2O_3$"–CaO–$SiO_2$ melts in air.

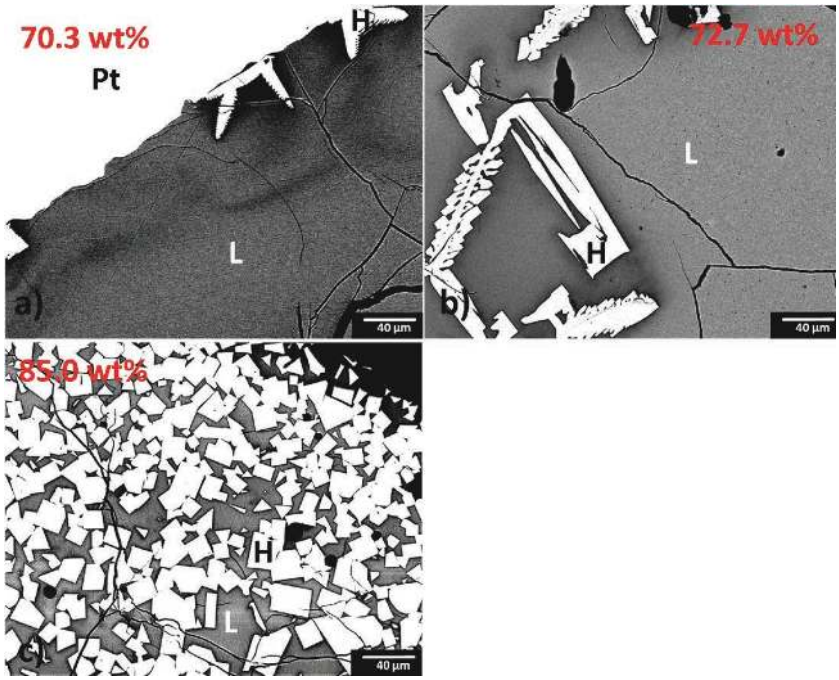


**Fig. 8.** Examples of typical microstructures observed in Assemblage I, sample cooled from 1 623 K (1 350°C) to 1 523 K (1 250°C) at 2 K/s with a $CaO/SiO_2$ = 3.46 wt/wt, containing a) 70.3 wt%, b) 72.7 wt% and c) 85.0 wt% $Fe_2O_3$ (L-liquid, H-Hematite) (BSE Micrograph). (Online version in color.)

to the formation for low (70.3 wt%) and medium (72.7 wt%) bulk $Fe_2O_3$ compositions.

The hematite was observed to form two types of crystals, faceted dendritic (skeletal) crystals at 70.3 wt% and 72.7 wt% bulk $Fe_2O_3$ concentrations and individual faceted crystals, typically euhedral equiaxed, at 85.0 wt% $Fe_2O_3$ in the bulk. At low bulk $Fe_2O_3$ concentrations, a larger proportion of hematite was observed to be present near the platinum substrate. Note the dendritic side arms are only formed in the 70.3 wt% and 72.7 wt% $Fe_2O_3$ samples. No side arms were observed to form on the hematite in the 85.0 wt% $Fe_2O_3$ samples despite cooling under the same conditions.

At 85 wt% $Fe_2O_3$ in the bulk, the hematite was relatively evenly distributed through the liquid. The crystals themselves were approximately 30 $\mu$m in width and length. It was confirmed experimentally that these crystals were present at the peak temperature of 1 623 K (1 350°C).

At 70.3 wt% and 72.7 wt% $Fe_2O_3$ in the bulk, the hematite was observed to be in the form of dendritic crystals, heterogeneously distributed throughout the liquid. With a decrease in hematite concentration from 72.7 wt% to 70.3 wt%, the temperature at which hematite nucleated and the proportion of hematite formed decreased. In addition, the length of the hematite crystals and dendrite arm length decreased, from 100 $\mu$m to 30 $\mu$m and from 10 $\mu$m to 4 $\mu$m respectively with decreasing from 72.7 wt% to 70.3 wt% $Fe_2O_3$ in the bulk.

Based on the melt composition along the $C_2S$-SFC boundary line at 1 508 K (1 235°C), estimated as the point at which Assemblage I transitions into Assemblage II, the proportion of hematite solidifying at this stage can be predicted. At a high (85.0 wt%) $Fe_2O_3$ bulk composition, it is estimated that at the end of the formation of Assemblage I the system contains 45.5 wt% liquid and 54.5 wt% hematite. At a 72.7 wt% and 70.3 wt% $Fe_2O_3$ bulk composition, it is estimated that the system contains 9.6 wt% and 17.4 wt% hematite respectively prior to the formation of Assemblage II.

### 3.3. Liquid + Hematite + $C_2S$ (Assemblage II)

Assemblage II is additive to Assemblage I, occurring with the nucleation and growth of $C_2S$. **Figure 9** shows micrographs typical of this phase assemblage.

For all bulk $Fe_2O_3$ compositions investigated, the $C_2S$ was observed in three phase assemblages, a thin layer on the individual hematite (IIa), individual $C_2S$ dendrites (IIb) and a coupled H–$C_2S$ microstructure (IIc) (See **Fig. 10**). The proportions of the three microstructures were observed to vary with bulk $Fe_2O_3$ composition. The proportion of the coupled H–$C_2S$ microstructure increased with a decreased bulk $Fe_2O_3$ concentrations, in agreement with the metastable H–$C_2S$ equilibrium and mass balances. The thickness of the thin $C_2S$ layer on the individual hematite (IIa) was not observed to vary with the bulk $Fe_2O_3$ composition. The fraction of this microstructure type (IIa) was typically proportional to the interfacial area of the hematite exposed to the melt.

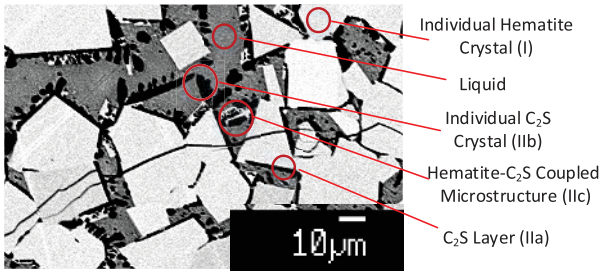


**Fig. 10.** Example of typical microstructures observed in Assemblage II (L+H+$C_2S$), sample cooled from 1 623 K (1 350°C) to 1 488 K (1 215°C) at 2 K/s and with a CaO/$SiO_2$ = 3.46 wt/wt, containing 85.0 wt% $Fe_2O_3$ (BSE Micrographs). (Online version in color.)

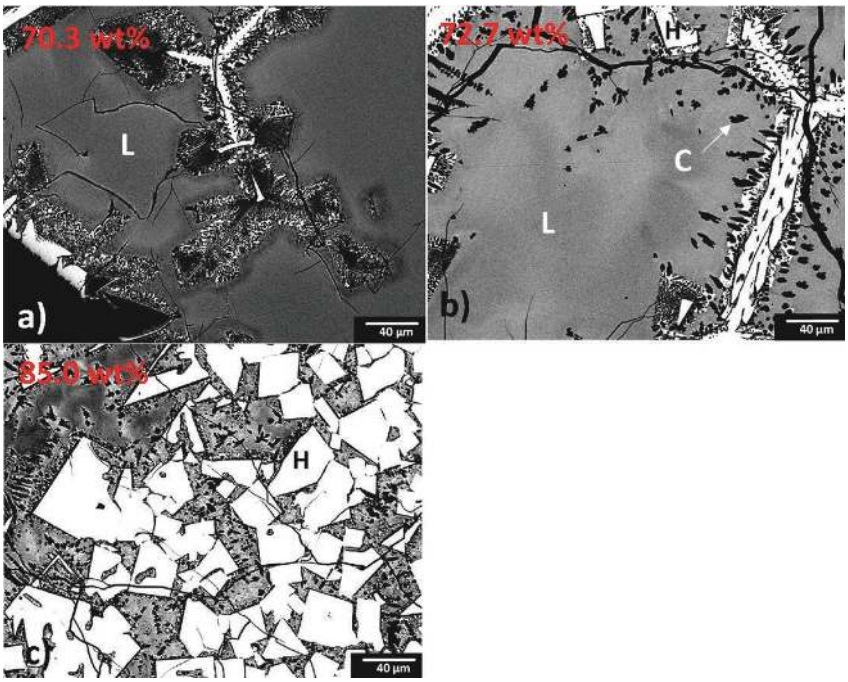


**Fig. 9.** Examples of typical microstructures observed in Assemblage II (L+H+$C_2S$), sample cooled from 1 623 K (1 350°C) to 1 493 K (1 220°C) at 2 K/s and with a CaO/$SiO_2$ = 3.46 wt/wt, containing a) 70.3 wt%, b) 72.7 wt% and c) 85.0 wt% $Fe_2O_3$ (L-liquid, H-Hematite, C–$C_2S$) (BSE Micrographs). (Online version in color.)

At 85.0 wt% $Fe_2O_3$ in the bulk, the $C_2S$ phase formed in the limited free volume between the hematite crystals. The $C_2S$ was observed to form all three microstructures, but due to the small free volume, the size of the $C_2S$ crystals was constrained. A larger number of individual $C_2S$ crystals (IIb) were observed to form, but of a smaller size, when compared to lower bulk $Fe_2O_3$ compositions.

At 70.3 wt% $Fe_2O_3$ in the bulk, the coupled H–$C_2S$ was either associated with the thin $C_2S$ layer (IIa) or individual $C_2S$ crystals (IIb), as illustrated by **Figs. 11** and **12**. The coupled H–$C_2S$ microstructure associated with the individual $C_2S$ crystals was observed to form in regions free of the individual hematite crystals.

### 3.4. Liquid + $C_2S$ + $CF_2$ (Assemblage III)

Phase assemblage III (L+$C_2S$+$CF_2$) was observed to form at all bulk $Fe_2O_3$ compositions, with two microstructures forming, individual $CF_2$ crystals (IIIa) and the coupled $C_2S$–$CF_2$ microstructure (IIIb) (See **Fig. 14**). The temperatures at which this phase assemblage was observed varied with the bulk $Fe_2O_3$ composition. **Figure 13** shows micrographs typical of this phase assemblage.

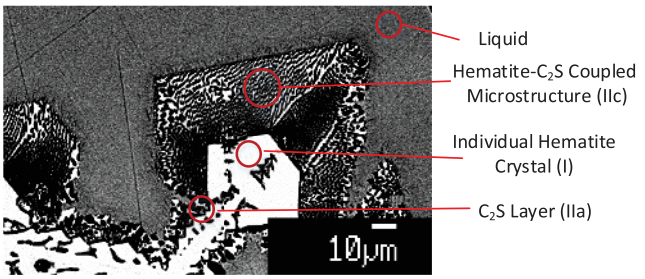


**Fig. 12.** Example of typical microstructures observed in Assemblage II, sample cooled from 1 623 K (1 350°C) to 1 498 K (1 225°C) at 2 K/s and with a $CaO/SiO_2$ = 3.46 wt/wt, containing 70.3 wt% $Fe_2O_3$. (BSE micrograph). (Online version in color.)

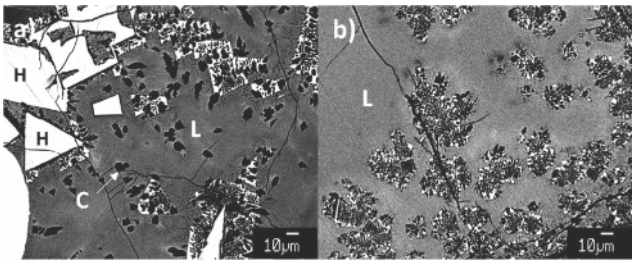


**Fig. 11.** Example of the two coupled $Fe_2O_3$–$C_2S$ microstructures (IIc), sample cooled from 1 623 K (1 350°C) to 1 498 K (1 225°C) at 2 K/s in air with 70.3 wt% $Fe_2O_3$ in the bulk and a $CaO/SiO_2$ = 3.46 wt/wt, the coupled H–$C_2S$-microstructure (IIb) associated with a) hematite (I) and b) individual $C_2S$ crystals (IIb) (L-liquid, H-Hematite, C–$C_2S$) (BSE Micrographs).

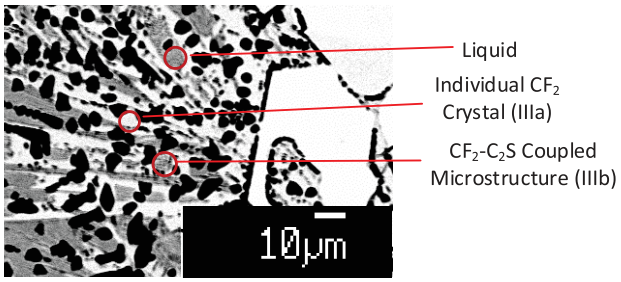


**Fig. 14.** Example of typical microstructures observed in Assemblage III (L+$C_2S$+$CF_2$), sample cooled at 2 K/s from 1 623 K (1 350°C) and a $CaO/SiO_2$ = 3.46 wt/wt with 85.0 wt% $Fe_2O_3$ (1 468 K, 1 195°C) (BSE). (Online version in color.)

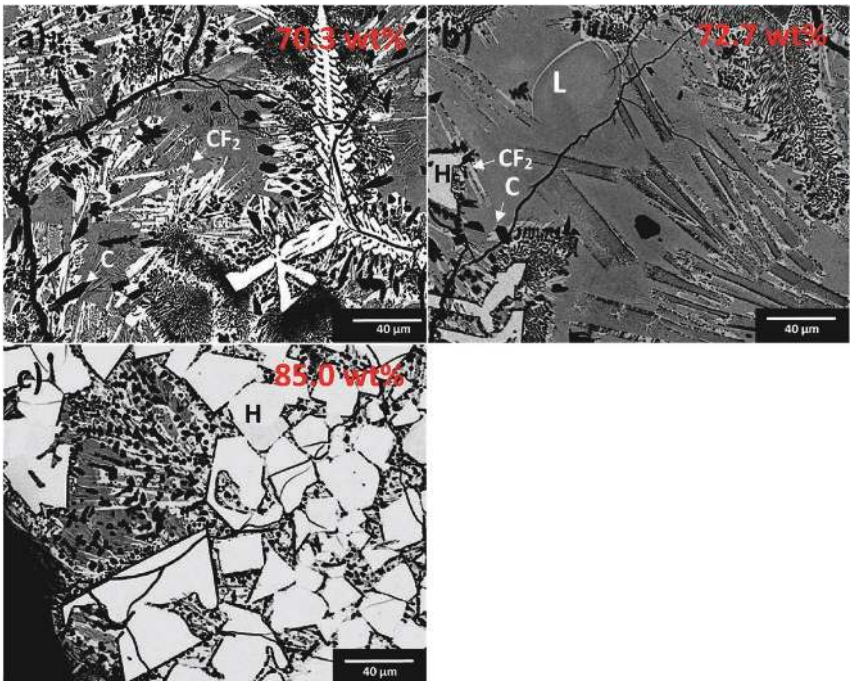


**Fig. 13.** Examples of typical microstructures observed in Assemblage III (L+$C_2S$+$CF_2$), sample cooled at 2 K/s from 1 623 K (1 350°C) and a $CaO/SiO_2$ = 3.46 wt/wt with a) 70.3 wt% $Fe_2O_3$ (1 463 K, 1 190°C), b) 72.7 wt% $Fe_2O_3$ (1 473 K, 1 200°C) and c) 85.0 wt% $Fe_2O_3$ (1 468 K, 1 195°C) (L-liquid, H-Hematite, C–$C_2S$, $CF_2$-Calcium Diferrite) (BSE Micrograph). (Online version in color.)

For all bulk $Fe_2O_3$ compositions, the individual $CF_2$ crystals were observed to be associated with the hematite, nucleating heterogeneously on this phase. The coupled $C_2S$–$CF_2$ (IIIb) microstructure was consistently observed to form on the individual $CF_2$ crystals. With a decrease in the bulk $Fe_2O_3$ composition, the proportion of liquid observed prior to the formation of $CF_2$ increased along with the proportion of $CF_2$ forming in assemblage III (see **Figs.** 14 and **15**).

As the proportion of $Fe_2O_3$ decreased in the bulk, the volume of the liquid phase from which $CF_2$ was able to form increased. This was associated with the observation of longer individual $CF_2$ crystals and a larger volume coupled $C_2S$–$CF_2$ (IIIb) microstructures. Similarly, the proportion of the coupled $C_2S$–$CF_2$ (IIIb) microstructure, relative to the other $C_2S$ containing microstructures, increased with decreasing bulk $Fe_2O_3$ concentration.

### 3.5. $C_2S$ + $CF_2$ + CF (Assemblage IV)

For all bulk $Fe_2O_3$ concentrations, individual CF crystals (IVa), coupled $C_2S$–CF (IVb) and a coupled $C_2S$–CF–$CF_2$ microstructure (IVc), were observed to form in Assemblage IV (see **Fig. 16**). The occurrence of the two CF containing coupled microstructures was confirmed via line analysis with EPMA. Assemblage IV is considered additive to both Assemblage III and Assemblage VI. Typical microstructures of this phase assemblage is shown in Fig. 16.

With a decrease in the bulk $Fe_2O_3$ concentrations, the proportion of liquid solidifying during the formation of Assemblage IV increased. A higher bulk $Fe_2O_3$ concentration resulted in smaller but more numerous crystals forming. The solids formed in this assemblage were constrained in shape and size by the solids that had formed at higher temperatures.

The proportion of CF solidifying as individual crystals was also observed to increase with an increase in the bulk $Fe_2O_3$ composition. At high bulk $Fe_2O_3$ compositions, the coupled microstructures were a smaller proportion of the solidified material in Assemblage IV.

### 3.6. Liquid + 'SFC-I' (Assemblage V)

This phase assemblage was only observed in the samples with a low bulk $Fe_2O_3$ concentration (70.3 wt% $Fe_2O_3$), forming at temperatures below 1 513 K (1 230°C). The 'SFC-I' was observed to form concurrently with Assemblage I, originating in regions free of hematite crystals, as illustrated in **Fig. 17**.

The phases present in the 'SFC-I' crystals were confirmed using XRD, with the phases confirmed through comparison with known XRD patterns for SFCA,[7] SFCA-I[8] and $Ca_{7.2}Fe^{2+}{}_{0.8}Fe^{3+}{}_{30}O_{53}$.[9] The XRD pattern, as shown in **Fig. 18**, indicated that the 'SFC-I' crystals consisted of both the SFC-I and $Ca_{7.2}Fe_{0.8}Fe_{30}O_{53}$ phases but no SFC (SFCA) is present. SFC-I and SFCA-I are considered to be structurally analogous, with the SFC-I an endmember of the SFCA-I solid solution series.

The 'SFC-I' individual crystals were observed to be

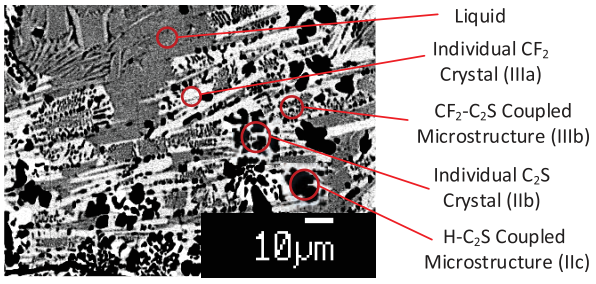


**Fig. 15.** Example of typical microstructures observed in Assemblage III (L+$C_2S$+$CF_2$), sample cooled at 2 K/s from 1 623 K (1 350°C) to 1 463 K (1 190°C) and a $CaO/SiO_2$ = 3.46 wt/wt with 70.3 wt% $Fe_2O_3$ (BSE). (Online version in color.)

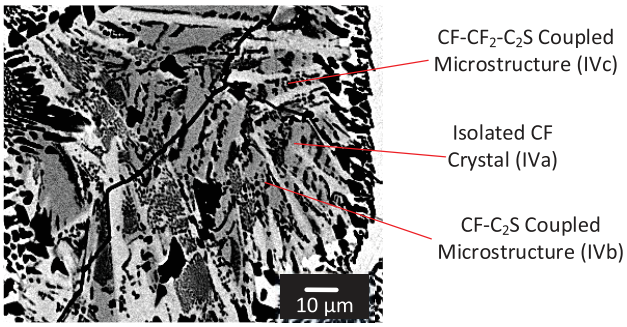


**Fig. 16.** Example of typical microstructures observed in Assemblage IV ($C_2S$+$CF_2$+CF), sample cooled at 2 K/s with a $CaO/SiO_2$ = 3.46 wt/wt with 70.3 wt% $Fe_2O_3$ (BSE). (Online version in color.)

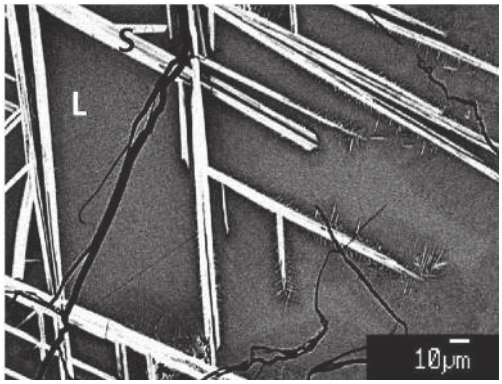


**Fig. 17.** Typical microstructure observed in Assemblage V (L+'SFC-I'), samples cooled from 1 623 K (1 350°C) to 1 498 K (1 225°C) at 2 K/s in air with 70.3 wt% $Fe_2O_3$ and a $CaO/SiO_2$ = 3.46 wt/wt (L-liquid, S-'SFC-I') (BSE Micrograph).

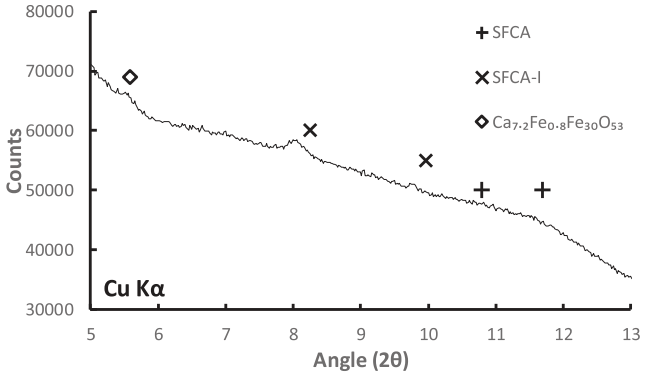


**Fig. 18.** XRD pattern obtained from material cooled from 1 623 K (1 350°C) to 1 073 K (800°C) at 2 K/s with 70.3 wt% $Fe_2O_3$ and a $CaO/SiO_2$ = 3.46 wt/wt in the bulk (Cu K$\alpha$).

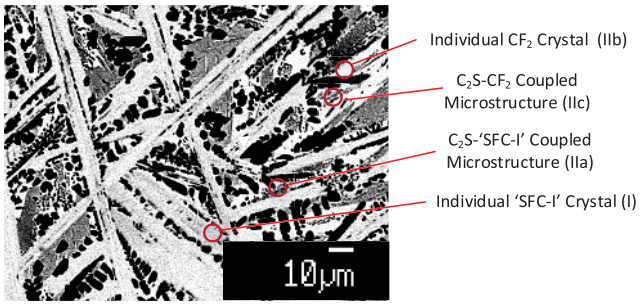


**Fig. 19.** Typical microstructures observed in samples cooled from 1 623 K (1 350°C) to 1 463 K (1 190°C) at 2 K/s in air with 70.3 wt% $Fe_2O_3$ and a $CaO/SiO_2$ = 3.46 wt/wt (BSE Micrograph). (Online version in color.)

distributed evenly in areas free of hematite, at least 100 $\mu$m from this phase. The 'SFC-I' crystals were consistently observed as single crystals, approximately 200 $\mu$m long and 10 $\mu$m wide, with branching side arms. The composition of the 'SFC-I' crystals were measured by EPMA, with the composition measured to be approximately 82.2 wt% $Fe_2O_3$, 2.9 wt% $SiO_2$ and 14.9 wt% CaO. Compared to that previously reported to form on cooling a liquid at 2 K/s with a $CaO/SiO_2$ ratio of 4.0 wt/wt and 69.24 wt% $Fe_2O_3$,[3] the bulk 'SFC-I' composition is higher in $SiO_2$ and the SFCA-I XRD peak is higher than the $Ca_{7.2}Fe_{0.8}Fe_{30}O_{53}$ peak. Based on the composition of the 'SFC-I' crystals, as measured by EPMA, the proportion of the silica free SFC-I in these crystals is 90% by mass, with the balance $Ca_{7.2}Fe^{2+}{}_{0.8}Fe^{3+}{}_{30}O_{53}$.

### 3.7. Liquid + $C_2S$ + 'SFC-I'/Liquid + $C_2S$ + $CF_2$ (Assemblage VI)

Assemblage VI was observed to form following Assemblage V, concurrently with Assemblage II. The two phase assemblages both required the nucleation and growth of $C_2S$. As previously reported,[3] four phase assemblages were observed, individual $C_2S$ crystals (VIa), coupled $C_2S$-'SFC-I' (VIb) individual $CF_2$ crystals (VIc) and coupled $C_2S$–$CF_2$ crystals (VId). **Figure 19** shows a micrograph illustrating this phase assemblage.

Using EPMA line analysis, as previously described,[3] the presence of the four microstructures was confirmed. The individual $C_2S$ crystals (VIa) appear to form on the individual SFC-I crystals or as isolated crystals in the liquid as unfaceted crystals (5 $\mu$m width and 30 $\mu$m length). The coupled $C_2S$-'SFC-I' microstructure (VIb) is observed in close association with the individual $C_2S$ crystals (VIa) and the individual 'SFC-I' crystals (V). The $C_2S$–$CF_2$ coupled microstructure (VId) was isolated from the SFC-I phase by unfaceted individual $CF_2$ crystals (VIc). Based on the occurrence and separation of the two coupled microstructures, the first coupled microstructure to form is the $C_2S$-'SFC-I' coupled microstructure (VIb), followed by the individual $CF_2$ crystals (VIc) and lastly the coupled $C_2S$–$CF_2$ microstructure (VId) in contact with the liquid.

## 4. Discussion

### 4.1. Formation of Assemblage I (L+H)

This phase assemblage was the first to be observed upon cooling the liquid. As the proportion of $Fe_2O_3$ in the bulk is increased, the temperature at which the phase assemblage was first observed increased. Consistent with the liquidus, at high $Fe_2O_3$ compositions (85.0 wt% $Fe_2O_3$), the hematite was present at the peak temperature 1 523 K (1 350°C), while for the samples with 70.3 wt% and 72.7 wt% $Fe_2O_3$ in the bulk, the hematite formed on cooling. Hematite formed on cooling was observed to be dendritic in structure, while that present at temperature was euhedral equiaxed.

At 85 wt% $Fe_2O_3$ in the bulk, the samples contained hematite at all stages, heating, peak temperature and cooling. As the sample were heated, the fine oxides reacted, melted and dissolved to form a homogenous liquid and hematite crystals. The hematite crystals were evenly distributed through the liquid, initially small in size. At temperature, the hematite crystals would have undergone grain growth via Ostwald ripening to decrease the surface free energy of the system. As such, the hematite crystals grew as individual faceted crystals rather than forming dendrites as observed at lower bulk $Fe_2O_3$ concentrations.

For samples heated above the liquidus, the hematite nucleated homogenously in the liquid or heterogeneously on the platinum wire or at the gas/liquid interface. With lower bulk $Fe_2O_3$ concentrations, the temperatures at which hematite nucleated decreased, leading to the initial formation and growth of dendrites occurring at lower temperatures. This in turn results in the formation of finer dendrite branches, due to a decrease in the rates of mass transfer in the liquid phase.

The proportion of hematite present at the conclusion assemblage I increased with increasing $Fe_2O_3$ in the bulk, impacting the formation of subsequent assemblages.

### 4.2. Formation of Assemblage II (L+$C_2S$+H)

Assemblage II is additive to Assemblage I, with new microstructures forming on the existing solids.[2] Analysis of the liquid compositions present in the later stages of Assemblage I shows that the melt is undercooled with respect to $C_2S$. Once nucleated, the $C_2S$ rapidly solidifies due to the supercooling, with a $C_2S$ layer (IIa) forming on the hematite followed by individual $C_2S$ crystals (IIb). Due to the rapid solidification of $C_2S$, moving the liquid composition directly away from the $C_2S$ composition and towards the $C_2S$-SFC boundary line. Solidification continues to occur with the formation of the coupled H–$C_2S$ microstructure (IIc), developing from the previously formed $C_2S$ crystals. The H–$C_2S$ structure is metastable since the SFC phase is not formed. At the final stages of this assemblage, the liquid composition has moved into the $CF_2$ primary phase field, becoming undercooled with respect to this phase.

Based on the melt composition at the SFC–$CF_2$–$C_2S$ invariant point,[6] taken as the point at which Assemblage II transitions into Assemblage III, the proportion of hematite and $C_2S$ at the end of the formation of assemblage III can be predicted. At a high (85.0 wt%) $Fe_2O_3$ bulk composition, it is estimated at the end of the formation of assemblage I the system contains 29.4 wt% liquid, 64.3 wt% hematite and 6.3 wt% $C_2S$. At a medium (72.7 wt%) and low (70.3 wt%) $Fe_2O_3$ bulk composition, it is estimated that the system contains 35.8 wt% and 29.5 wt% hematite respectively and 11.5 wt% and 12.5 wt% $C_2S$ respectively, prior to the formation of Assemblage III.

At high $Fe_2O_3$, the $C_2S$ was observed to primarily form as individual $C_2S$ crystals (IIb). This microstructure is associated with hematite, suggesting that increasing the proportion of hematite increases the probability of $C_2S$ nucleation at higher temperatures. The individual $C_2S$ crystals were constrained by the existing hematite solids, limiting the length of the dendrites formed. The limited free volume for solidification and the short distance between $C_2S$ and hematite, increased the likelihood of the divorced solidification of $C_2S$ and hematite rather than the coupled solidification of $C_2S$ and hematite.

With a decrease in the bulk $Fe_2O_3$ concentrations, the proportion of $C_2S$ forming in the initial stages of solidification increased. However, due to the limited solidification of hematite in Assemblage I, there was a decrease in the surfaces on which $C_2S$ was able to nucleate in association with. Both of these factors were potential contributors to the formation of $C_2S$ dendrites in the liquid. At low bulk $Fe_2O_3$ concentrations, the proportion of the coupled $C_2S$-hematite microstructure increased.

### 4.3. Formation of Assemblage III ($L+C_2S+CF_2$)

Assemblage III consisted of individual $CF_2$ crystals (IIIa) and a coupled $C_2S$–$CF_2$ microstructure (IIIb), with formation occurring in that order. The individual $CF_2$ crystals (IIIa) heterogeneously nucleated on hematite, occurring in a liquid undercooled with respect to $CF_2$. The $C_2S$–$CF_2$ coupled microstructure (IIIb) subsequently formed, with solidification of this coupled microstructure moving the liquid composition along the $C_2S$–$CF_2$ boundary line and towards the ternary $C_2S$–$CF_2$–CF eutectic invariant point.

With the variation of $Fe_2O_3$ in the bulk, the proportion of material solidifying in Assemblage III and the resulting microstructures are changed. Assuming that the melt composition at the end of the formation of Assemblage II coincided with the SFC–$C_2S$–$CF_2$ ternary invariant point (1 215°C, 1 488 K) and the end of the formation of Assemblage III coincided with the $C_2S$–$CF_2$–CF ternary invariant point(1 192°C, 1 465 K), the proportion of melt solidifying can be calculated. At a bulk $Fe_2O_3$ concentration of 85.0 wt%, the liquid present decreased from 29.4 wt% to 19.3 wt% of the bulk as a result of the formation of Assemblage III. Similarly, the proportion of liquid present in samples with 70.3 wt% and 72.7 wt% $Fe_2O_3$ in the bulk decreased from 53.1 wt% to 34.8 wt% and 58.0 wt% to 38.0 wt% respectively between the two invariant points.

With an increase in $Fe_2O_3$ in the bulk from 70.25 wt% to 85.0 wt%, the proportion of material solidified in Assemblage III decreased from 20 wt% to 10 wt%. This resulted in a decrease in the size of the $CF_2$ crystals and the proportion of the coupled $C_2S$–$CF_2$ microstructure. The $CF_2$ crystals were constrained by the previously solidified material, reducing the size to which they could grow.

With a decrease in the bulk $Fe_2O_3$ concentration, the proportion of coupled $C_2S$–$CF_2$ relative to individual $CF_2$ crystals increased. This indicates that under these conditions that the divorced solidification of $C_2S$ and $CF_2$ was less favourable than coupled solidification. This is potentially as a result of the long distances over which diffusion was required for solidification to occur.

### 4.4. Formation of Assemblage IV ($C_2S+CF_2+CF$)

The formation of assemblage IV is considered additive to both assemblage III and VI. The formation of assemblage IV comprises of three steps. Individual crystals of CF (IVa) formed first, solidifying from a liquid undercooled with respect to CF. This was followed by the formation of the $C_2S$–CF coupled microstructure (IVb), which forms via a coupled growth mechanism. Finally the $C_2S$–$CF_2$–CF coupled microstructure (IVc) occurs, solidifying the remaining liquid as a ternary eutectic.

As with assemblage III, the variation of $Fe_2O_3$ in the bulk resulted in a change in the proportion of material solidifying in this phase assemblage. An increase in $Fe_2O_3$ in the bulk resulted in the decrease in the proportion of material solidifying in assemblage IV. This led to a decrease in the size of the CF crystals and the proportion of the coupled $C_2S$–CF and $C_2S$–CF–$CF_2$ microstructures relative to the total.

### 4.5. Formation of Assemblage V (L+'SFC-I')

During the solidification of hematite at a low (70.3 wt%) bulk $Fe_2O_3$ concentration, 'SFC-I' was observed to nucleate homogenously in regions free of hematite. This resulted in the occurrence and formation of Assemblage V. These crystals formed during the solidification of hematite in Assemblage I, with the two assemblages (I and V) forming in separate regions of the samples and following different solidification pathways as illustrated in Fig. 7. As previously reported,[3] the individual 'SFC-I' crystals appear to form through heterogeneous nucleation on the platinum substrate and at the liquid-gas interface and later homogenously in the liquid. Once nucleated, the 'SFC-I' crystals grow as the temperature is decreased, with the number of 'SFC-I' crystals increasing with decreasing temperature through subdivision and heterogeneous nucleation on existing 'SFC-I' crystals. The individual 'SFC-I' crystals appear to be in the form of intergrowths of SFCA-I and $Ca_{7.2}Fe^{2+}_{0.8}Fe^{3+}_{30}O_{53}$. The 'SFC-I' continued to solidify until the liquid was undercooled with respect to $C_2S$.

Based on the concurrent formation of two separate Assemblages in separate regions, it appears that the heterogenous homogenous nucleation of the 'SFC-I' is unlikely to occur in close proximity to hematite. The two phases, hematite and 'SFC-I', both in a metastable state yet continue to form on cooling under the same conditions.

### 4.6. Formation of Assemblage VI ($L+C_2S+$'SFC-I'/ $L+C_2S+CF_2$)

Assemblage VI was only observed in the samples with a low (70.3 wt%) bulk $Fe_2O_3$ concentration. The formation of this phase assemblage is dependent on the prior formation of Assemblage V. As such, the proportion of Assemblage VI will increase under conditions that favour the formation of Assemblage V.

This phase assemblage is considered additive to Assemblage V and independent of Assemblage I, II and III. It suggested that this phase assemblage formed in two stages, first $C_2S$–SFC–I solidification and second $C_2S$–$CF_2$ solidification.

### 4.7. Overall Impacts of the Bulk $Fe_2O_3$ Compositions on Solidification

The results of the current study have demonstrated that

the proportion of $Fe_2O_3$ in the bulk has a significant impact on the phases, assemblages and microstructures present when oxide liquids are solidified. While the process conditions were identical for the three bulk $Fe_2O_3$ compositions examined, the proportion and appearance of the phase assemblages varied. Consistent with previous research,[2,3] the phase assemblages formed are significantly differs from those formed under equilibrium and Scheill-Gulliver cooling.

In the system investigated, it has been demonstrated that the bulk $Fe_2O_3$ composition influenced the morphology and proportion of the hematite phase formed during the initial stages of solidification. When hematite is present at the peak temperature, the crystals were observed to be euhedral equiaxed, as opposed to forming dendritic structures when formed on cooling. With an increase in the bulk $Fe_2O_3$ concentration, the proportion of hematite crystals present in the microstructures increased as did the size and number of crystals.

The hematite phase, which is retained as a metastable phase on cooling, was also observed to influence the solidification of subsequent microstructures. Increasing the concentration of hematite in the bulk resulted in an increase in the proportion of hematite present and a decrease in the volume of the liquid phase from which subsequent microstructures were formed. This led to a decrease in the proportion of coupled microstructures compared to the individual crystals.

A decrease in the volume fraction of hematite formed during cooling was associated with the formation of SFCA-I and $Ca_{7.2}Fe_{0.8}Fe_{30}O_{53}$ in regions free of hematite. Based on this observation, it is suggested that the nucleation of SFCA-I and SFCA is unlikely occur in close proximity to hematite. This observation provides a valuable insight into the impact of $Fe_2O_3$ variation, both within the bulk material and due to the heterogeneity of the sintered material, on the microstructures formed.

## 5. Summary

The effects of changes to the bulk $Fe_2O_3$ concentration on the solidification processes and microstructures formed on cooling liquids in the "$Fe_2O_3$"–CaO–$SiO_2$ system in air have been determined in the high $Fe_2O_3$ region of this system.

Samples of a bulk composition with a CaO/$SiO_2$ ratio of 3.46 and 70.3 wt%, 72.7 wt% and 85.0 wt% $Fe_2O_3$ were cooled at 2 K/s from 1 623 K (1 350°C) to 1 453 K (1 180°C). The phases formed and processes occurring during cooling were identified and have been shown to differ from those predicted under equilibrium cooling. The phases formed were, in order of formation, hematite ($Fe_2O_3$), dicalcium silicate ($Ca_2SiO_4$), calcium diferrite ($CaFe_4O_7$) and calcium ferrite ($CaFe_2O_4$). At low bulk $Fe_2O_3$ compositions (70.3 wt%), SFCA-I and $Ca_{7.2}Fe^{2+}{}_{0.8}Fe^{3+}{}_{30}O_{53}$ were also observed to form at selected conditions. The SFC phase did not form on cooling these materials.

The proportion of $Fe_2O_3$ in the bulk melt is shown to influence the proportion of hematite in the final structure and the morphology of the hematite phase formed on cooling. The changes in the proportion of metastable hematite formed changes the proportion of liquid present at any temperature, the proportion of other phases present and the microstructures present in the final material. With a decrease of the bulk $Fe_2O_3$ concentration, the proportion of hematite formed on cooling decreased and the proportion of coupled microstructures relative to individual crystals increased. At low bulk $Fe_2O_3$ compositions, the SFCA-I and $Ca_{7.2}Fe^{2+}{}_{0.8}Fe^{3+}{}_{30}O_{53}$ phases were observed to form in regions free of hematite.

**Acknowledgements**

The authors would like to thank the Australian Research Council Linkage grant scheme and BHP for financial support to enable this research to be carried out, and to the Centre of Microstructure and Microanalysis (CMM), the University of Queensland for providing electron microscope facilities that enabled the microanalytical measurements to be undertaken. This research was supported by an Education Endowment Fund (EEF) scholarship from the Australasian Institute of Mining and Metallurgy (AusIMM) and an Australian Government Research Training Program (RTP) Scholarship.

## REFERENCES

1) J. Ostwald: *BHP Tech. Bull.*, **25** (1981), 13.
2) S. Nicol, E. Jak and P. Hayes: *Metall. Mater. Trans. B*, **50** (2019), 2706.
3) S. Nicol, E. Jak and P. Hayes: *Metall. Mater. Trans. B*, **50** (2019), 3027.
4) S. Nicol, E. Jak and P. Hayes: *ISIJ Int.*, **60** (2020), 865.
5) S. Nicol, J. Chen, W. Qi, X. Mao, E. Jak and P. Hayes: *Minerals*, **9** (2019), 374.
6) J. Chen, M. Shevchenko, P. Hayes and E. Jak: *ISIJ Int.*, **59** (2019), 795.
7) J. Hamilton, B. Hoskins, W. Mumme, W. Borbidge and M. Montague: *Neues Jahrb. Mineral., Abh.*, **161** (1989), 1.
8) W. Mumme, J. Clout and R. Gable: *Neues Jahrb. Mineral., Abh.*, **173** (1998), 93.
9) H. Hughes, P. Roos and D. C. Goldring: *Mineral. Mag. J. Mineral. Soc.*, **36** (2018), 280.